

## SYNTHESIS OF EOSIN Y-SENSITIZED Ag-TiO<sub>2</sub> NANO-HYBRID FOR OPTIMIZED PHOTOCATALYTIC DEGRADATION OF AQUEOUS CAFFEINE

MUKTAR MUSA IBRAHIM<sup>a</sup>, UMAR IBRAHIM GAYA<sup>1a</sup>

<sup>a</sup>Department of Pure and Industrial Chemistry, Faculty of Physical Sciences, Bayero University, Kano, 700241 Kano, P.M.B. 3011, Kano State, Nigeria

### ABSTRACT

The visible light spectral response of titania nanoparticles synthesized by hybrid treatment of TiO<sub>2</sub> with silver dopant and Eosin Y-sensitizer was evaluated using caffeine, an emerging pollutant. The photocatalyst was characterized using scanning electron microscopy (SEM), x-ray diffraction (XRD), solid state UV/Visible spectrometry and Fourier transform infrared spectrometry (FTIR). Upon sensitization and doping, downsizing, increase in surface area and redshift were observed without significant annihilation of the tetragonal anatase and rutile structures. Factors affecting the degradation of caffeine were studied using Taguchi orthogonal array model and optimized using a response surface methodology (RSM) based on faced-centered composite design (FCCD). Caffeine degradation under the conditions of the study was not affected significantly by temperature but pH, initial concentration and catalyst concentration. Evidence for electron injection and red shift with sensitization was corroborated using quantum calculations at DFT/B3LYP level of the theory.

**Keywords:** TiO<sub>2</sub>; Photocatalysis; Caffeine; Taguchi; RSM; Doping.

### 1. INTRODUCTION

The past few decades have seen increasing concern over the presence of pharmaceuticals in aquatic environment. Caffeine is a naturally occurring purine alkaloid used in coffee, tobacco and tea as an analeptic<sup>1</sup>, and as enhancer in certain analgesics. This psychoactive substance is now recognized as emerging pollutant<sup>2</sup> due to its endocrine disrupting property, recalcitrance and ubiquitous presence in aquatic environment<sup>3,4</sup>. The removal of caffeine by adsorption<sup>5,6</sup> and biodegradation<sup>7</sup>, has been achieved. These methods are however characterized by non-destructiveness and slow rate of removal.

Advanced oxidation Technologies (AOTs) driven by in-situ generated hydroxyl radicals, are now being intensively investigated due to their capacity for total oxidation of pollutants. By far, the removal of caffeine by AOTs such as ozonation, non-thermal plasma<sup>8</sup> electro-Fenton and other Fenton-based oxidation methods, have been demonstrated<sup>9,10</sup>. However, the electrochemical and non-thermal plasma methods have the disadvantage of being energy intensive, and Fenton and photo-Fenton processes are predisposed to extreme pH dependence<sup>11</sup>. Accordingly, even though ozonation performed singly or in combination with other methods, has been effective in the removal of certain pharmaceuticals<sup>12</sup>, poor performance has been reported in the case of caffeine<sup>13,14</sup>. Rosal et al.<sup>15</sup> found the ozonation of caffeine was especially rapid during the initial stage of the reaction period but declines thereafter to a much slower rate.

Among AOTs, photocatalysis has recorded significant success in effective caffeine removal. The process involves the utilization of holes and hydroxyl radicals harvested from sufficiently light-excited photoresponsive catalyst<sup>16</sup>. A few photocatalytic degradation studies on caffeine relied on TiO<sub>2</sub> which has been considered to be chemostable and effective<sup>17</sup>. Nevertheless, large scale photocatalytic degradation is challenged by the inability of TiO<sub>2</sub> to effectively absorb light in the visible region of the solar spectrum<sup>18</sup>, hence the search for visible light responsive catalysts or improved titania preparations.

Dye-sensitization and doping constitute two prominent (coupling and band-gap modification) methods that successfully bridged this gap. In the latter, dye molecule is excited to produce electron which can be easily injected to the conduction band of the semiconductor for oxidation of oxygen molecule to superoxide (O<sub>2</sub><sup>•-</sup>) and hydroperoxide (OOH<sup>•</sup>) and hydroxyl radicals<sup>19</sup>. Dye-sensitization has been effective in various applications such as selective oxidation of alcohols<sup>20</sup>, photocatalytic degradation<sup>21</sup> and solar cell<sup>22</sup>. Similarly, the visible light photoactivity of Ag-doped TiO<sub>2</sub> has been established and dye sensitized coupled systems have been reported<sup>23,24</sup>. In this study, Eosin Y (EY) which was variously found to be an excellent sensitizer<sup>8,25</sup> is applied to Ag-doped TiO<sub>2</sub> for the degradation of caffeine. The factors affecting degradation were optimized with the aid of Taguchi and face-centered central composite design. Changes in electronic absorption spectra of EY functionalized Ag-TiO<sub>2</sub> via a carboxylate bridge was studied by the application of density functional theory (DFT) using hybrid functional (B3LYP).

### 2. EXPERIMENTAL

#### 2.1 Chemicals

Titanium dioxide (99.5 %) and H<sub>2</sub>SO<sub>4</sub> (98.08 %) were purchased from Loba Chemie, India. Eosin Y dye (99 %) was supplied by Sigma Aldrich, Canada. Silver nitrate (90 %), caffeine (99 %) and NaOH (98 %) were obtained from BDH, Poole, England. All chemicals were used as received from the manufacturers without further purification. Stock solutions were prepared using deionizer distilled water and used fresh. All experiments were carried out in a 30 cm long, 1L capacity, round bottom batch photoreactor previously described<sup>26</sup>, maintained at 299 K. The visible light source was a W-lamp having luminous flux of 5250 lm. This lamp was jacketed in cylindrical quartz glass of 7 cm diameter dipping down the reactor bottom. The effective volume of the photoreactor was 0.6 L. The structure of caffeine and EY are shown in Fig. 1.

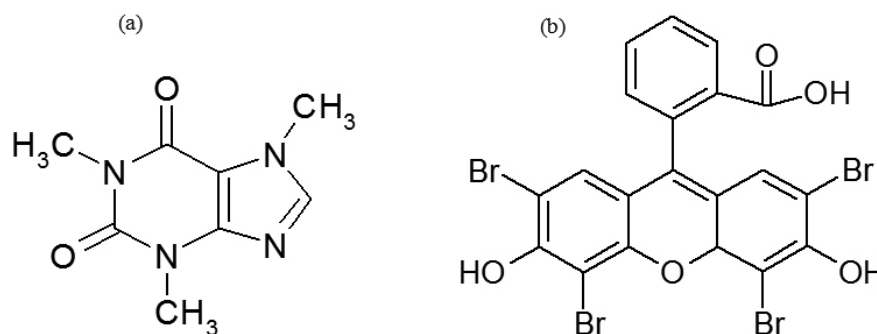


Fig. 1: Molecular structures of caffeine (a), and EY (b), used in the study.

### 2.2 Synthesis of EY/Ag-TiO<sub>2</sub> photocatalyst

The doping of TiO<sub>2</sub> with Ag was carried out using the photodeposition method reported by Wen et al.<sup>27</sup>. Specifically, TiO<sub>2</sub> (5.0g) and AgNO<sub>3</sub> (0.3-2.1% mole ratio versus TiO<sub>2</sub>) were added into 100 ml distilled water and was acidified using dilute H<sub>2</sub>SO<sub>4</sub>. The mixture was then stirred continuously under irradiation by a 25 W mercury lamp for 1 hour. The resulting precipitate was dried in oven for 12 h at 100 °C, ground and calcined at 400 °C for 4 hours and dried to obtain Ag-TiO<sub>2</sub>. In order to sensitize this material, 1g of the Ag-TiO<sub>2</sub> powder was transferred into a round bottom flask containing 0.1 M ethanolic solution of the EY. The pH of the resulting suspension was adjusted to 7 using H<sub>2</sub>SO<sub>4</sub> and NaOH (0.5 M solutions) and the mixture was refluxed at 80 °C for 2 h so as to effectively bind the dye onto the Ag-TiO<sub>2</sub>. The emerging solid fraction was filtered, washed three times with deionized water and 95 % ethanol and then stored in dark container to avoid deactivation.

### 2.3 Photocatalyst characterization

In order to determine the crystal properties of the prepared titania catalysts, X-ray diffraction was performed using Philips X'Pert Pro diffractometer, using Cu-Kα source (λ = 1.56877 Å). The diffractometer was operated at 30 kV and 30 mA, over a 2θ range of 20° to 120°. Morphology of the catalysts was recorded on LEICA stereo scan - 440 interfaced with Phoenix proxy energy dispersive x-ray spectrometer. The FTIR spectra of the blank catalyst and dye sensitized was recorded using Agilent Cary 630 diamond attenuated total reflectance Fourier transform infrared spectrometer (ATR-FTIR). Band gap was calculated from electronic data recorded on Lambda 35 Perkin Elmer UV/Vis spectrophotometer using Schuster-Kubelka-Munk relations. Spectrum was scanned over wavelength range of 200 to 800 nm.

### 2.4 Photocatalytic experiments

In each experimental run, 400 ml aqueous solution of desired amount of caffeine and EY/Ag-TiO<sub>2</sub> photocatalyst were added to the photoreactor and the pH of the suspension was adjusted using 0.5M NaOH and H<sub>2</sub>SO<sub>4</sub>. Aliquot was consistently taken at 0, 30, 50, 70, 90, 110, 130, 150, 170, 190, 210, 230, 250, 270 and 290 min, which was centrifuged for 20 min at 1500 rpm. The supernatant liquid obtained was then filtered using 0.45 μm cellulose nitrate filter. Residual caffeine levels were monitored by measuring absorbance at 271.56 nm using Perkin Elmer Lambda 25 UV-visible spectrophotometer. The percentage degradation efficiency was calculated as percent (% D) of the initial caffeine concentration using Eq. 1.

$$\%D = \frac{[Caffeine]_0 - [Caffeine]_t}{[Caffeine]_0} \times 100 \quad (1)$$

Where [Caffeine]<sub>0</sub>= initial caffeine concentration, [Caffeine]<sub>t</sub> = concentration of caffeine at irradiation time *t*.

### 2.5 Optimization and kinetic profiling

To optimize the photocatalytic degradation of caffeine, a three-level, three-variable, non-rotatable, face-centered central composite design (FCCD) was employed. The independent parameters were the pH (A), EY/Ag-TiO<sub>2</sub> concentration (B) and initial caffeine concentration (C) in three levels (low, central, high) and three codes (-1, 0, +1) as displayed in Table 1. In this FCCD, a total of 20 experiments (N) were performed including 6 centre experiments as guided by the formula N = 2<sup>n</sup> + 2n + 6. Where n is the number of variables. Other variables such as agitation speed, light intensity, oxygen pressure and delivery volume were kept constant. The degradation efficiencies obtained from experiments were processed using Design Expert v6 to obtain the caffeine degradation model. In order to find the kinetic scheme consistent with the degradation of caffeine on EY/Ag-TiO<sub>2</sub>, experiments were run at optimal operating conditions and data were fitted into integrated rate equations. The profiles of possible background reactions such as adsorption on bare TiO<sub>2</sub> and photolysis in absence of TiO<sub>2</sub> were also examined. These were compared with photocatalysis over EY-TiO<sub>2</sub>, Ag-TiO<sub>2</sub>, EY/Ag-TiO<sub>2</sub>.

**Table 1:** Operating variables, levels and their codes.

Experimental variables	Notation (and unit)	Levels (and codes)		
pH	A	3.0(-1)	5.5(0)	8.0(+1)
Catalyst dose	B (g/L)	1.00(-1)	1.75(0)	2.50(+1)
Caffeine concentration	C (mg/L)	10(-1)	30(0)	50(+1)

### 2.6 Effect of operating parameters

The effect of parameters was studied using four associated variables (initial caffeine concentration, catalyst dosage, pH and temperature) with minimum number of experiments, a three-levels-four-factor Taguchi orthogonal array (OA) L<sub>9</sub> (3)<sup>4</sup> design was performed using Minitab 17 statistical software package. Nine degradation experiments were conducted at three experimental levels (1, 2, and 3) of each parameter. The experimental factors with the strongest influence on the degradation of caffeine were determined based on the value of signal to noise ratio, and p-value. The experimental parameters and levels used for the Taguchi design are shown in Table 2.

**Table 2:** Experimental factors, levels and codes as used for the Taguchi design.

Code	Experimental variables	Levels in coded form			Units
		1	2	3	
A	Catalyst Dosage	1	1.5	2	g/L <sup>-1</sup>
B	pH	3	6	8	-
C	Temperature	35	45	65	°C
D	Caffeine Concentration	10	30	50	mg/L

### 2.7 Quantum chemical calculations

All calculations were performed using Gaussian 09 program. The ground state geometries were optimized at DFT/B3LYP level of theory using a standard 6-316(d) basis set. The excitation energies and oscillator strength (*f*) for singlet-singlet transition at optimized geometry by DFT calculations using the same hybrid functional and basis set.

### 2.8 Catalyst characterization using XRD

Rietveld profile refinement of the structures was performed using WINPLOTR package of FullProf suite version 3.0. The average crystalline size of EY-sensitized TiO<sub>2</sub> and regular TiO<sub>2</sub> photocatalyst were calculated using Williamson-Hall (Eq. 2) and the Scherer equation (Eq. 3). With the former, crystallite sizes were calculated from the y-intercept of the plot of β cos θ against Sinθ while the strain (ε) was calculated from the slope.

$$\beta \cos \theta = \frac{K \lambda}{size} + 4 \epsilon \times \sin \theta \quad (2)$$

$$Crystallite\ size = \frac{K \lambda}{\beta \cos \theta} \quad (3)$$

Where *K* is a constant 0.891, λ is the wavelength of X-ray radiation, β is the full width at half maximum intensity (FWHM) in radians, θ is diffraction angle at the position of peak maximum. Anatase and rutile contents of the titania photocatalysts were calculated using Spurr-Myers equation (Eq. 4)<sup>28</sup> as it has been widely found applicable<sup>29,30</sup>.

$$w_A = \frac{1}{1 + 1.26 \frac{I_R}{I_A}} \quad (4)$$

Where *w<sub>A</sub>* is the weight fraction of the anatase polymorph, *I<sub>R</sub>* is the intensity of diffraction peak for rutile and *I<sub>A</sub>* is the intensity of diffraction peak for anatase.

The lattice parameters (a, b and c) of EY/Ag-TiO<sub>2</sub> photocatalyst were calculated using equation (5). The calculated values for the anatase and rutile polymorphs of the EY-Ag/TiO<sub>2</sub> photocatalyst were compared to the unit cell parameters for standard anatase (JCPDS card no. 21-1272) and rutile (21-1276) polymorphs of TiO<sub>2</sub>.

$$\frac{1}{d^2} = \frac{h^2 + k^2}{a^2} + \frac{l^2}{c^2} \quad (5)$$

Where *d* is the spacing between planes in atomic lattice. The *h*, *k* and *l* are the miller indices, while *a*, *b* and *c* are lattice parameters.

### 3.0 RESULTS AND DISCUSSION

#### 3.1 Photocatalyst characterization

##### 3.1.1 XRD analysis

Crystallite size and structure of materials constitute important factors that can dictate the efficiency of photocatalyst. An overlay of the diffraction profiles of the EY/Ag-TiO<sub>2</sub> and regular TiO<sub>2</sub> photocatalyst are displayed in Fig. 2. The sensitized TiO<sub>2</sub> material shows anatase peaks at 2θ (and planes) = 25.88°(101), 39.47°(004), 46.72°(200), 73.87° (215) and rutile peaks (and planes) at 27.02°(110), 39.47° (111), 54.46°(211), 64.03°(310). Even though XRD pattern of photodeposited silver on TiO<sub>2</sub> does not modify the crystal structure of TiO<sub>2</sub>, so does not usually show metallic silver peaks corresponding to planes 111(39.76°) and 220(67.71°)<sup>27, 31,32</sup> presumably due to being below visibility limit of XRD<sup>33</sup>, the presence metallic silver is herein evidenced by the presence of a prominent diffraction peak at 34.12° corresponding to Ag(111) reflection. The bare TiO<sub>2</sub> (Fig. 2) displayed strong anatase peaks at 38.26°(004), 48.49°(200), 69.11°(116) 75.44°(215), and rutile peaks at 41.72°(111), 54.33°(211) and 63.09°(002). The rutile and anatase peaks and planes correspond to those of pure phases reported in literature<sup>34,35</sup>.

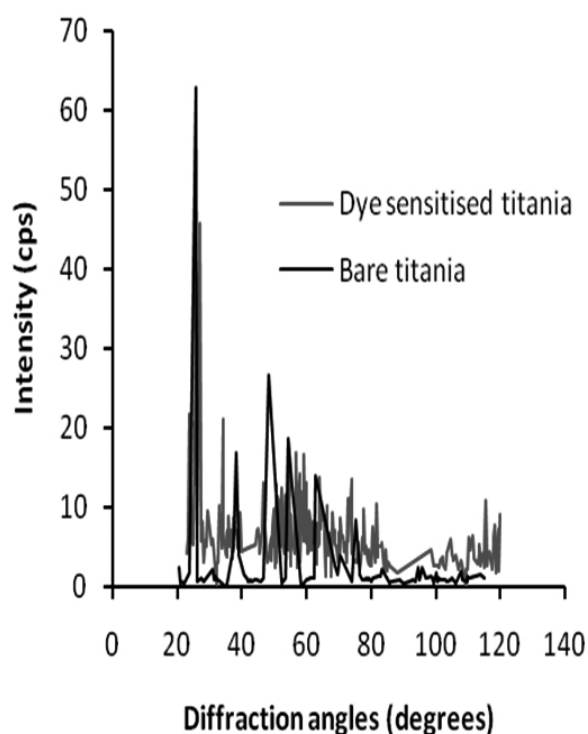


**Fig. 2:** Overlay of diffractograms showing XRD peaks of EY/Ag-TiO<sub>2</sub> (coloured red) and bare TiO<sub>2</sub>(black).

**Table 4:** Particle size estimated using Debye Scherer and Williamson-Hall methods.

Catalyst	Particle size (nm)		Polymorphs (%)		Specific surface area (m <sup>2</sup> g <sup>-1</sup> )
	Debye-Scherer	Williamson-Hall	Anatase	Rutile	
TiO <sub>2</sub>	79.1	138.64	97.6	2.32	24.32
EY-Ag/TiO <sub>2</sub>	58.3	69.32	73.9	ca 26.1*	17.92

\*The rutile content depends on the amount of amorphous TiO<sub>2</sub> possibly present.

The unit cell parameters of the EY-sensitized Ag-TiO<sub>2</sub> were calculated (Table 3) based on anatase lattice planes 101 and 004 and rutile reflections 111 and 211. It would be seen that the values displayed in Table 3 agree with the standard lattice parameters for pure anatase (a= 0.3784 nm and c = 0.9515 nm) and pure rutile (a = 0.4536 nm and c = 0.29587 nm)<sup>37</sup>. This confirms that the EY/Ag-TiO<sub>2</sub> contains a mixture of anatase and rutile polymorph in their tetragonal structures. The crystal structure properties of the EY/Ag-TiO<sub>2</sub> and regular TiO<sub>2</sub> are shown in Table 3. Rietveld analysis of the diffraction data showed the exclusive presence of only the anatase and rutile peaks in the bare TiO<sub>2</sub>. The mass percentages of anatase and rutile polymorphs in the regular TiO<sub>2</sub> were 97.6 and 2.32 %, respectively. Basically, mixture of anatase and rutile TiO<sub>2</sub> polymorphs has been reported to have superior photocatalytic ability than either polymorph in its pure form as it is in the case of the popular Degussa P-25 with 70-80 % anatase and rutile rest<sup>36,38</sup>. The XRD profile of EY-sensitized Ag-TiO<sub>2</sub> (Fig. 2) shows amorphousness resulting from the sensitization with 73.9% anatase, and 26.1 % distributed among rutile and amorphous material. Unless an isolation of the polymorphs is performed, it will be erroneous to rule out the presence of amorphous TiO<sub>2</sub><sup>38</sup>.

**Table 3:** Crystal structure properties of the as-synthesised EY/Ag-TiO<sub>2</sub>.

Property	EY/Ag-TiO <sub>2</sub>	
	Anatase unit	Rutile unit
Crystal structure	Tetragonal	Tetragonal
Lattice structure (nm)	a = 0.370	a = 0.453
	c = 0.947	c = 0.295
Unit cell volume (nm <sup>3</sup> )	0.136	0.258

The average crystallite size of the EY/Ag-TiO<sub>2</sub> was calculated using Scherer equation. Because values obtained (Table 4) were slightly above the level which particles are expected to show strain (<50 nm), values were also calculated from more suited Williamson-Hall profile (supplementary materials, Fig. A-1 and Fig. A-2). In both cases, downsizing of the TiO<sub>2</sub> particles was observed after sensitization, which may be attributed to large degree of distortions<sup>39</sup>. The Williamson particle size dropped from 138 nm to 69.32 nm.

##### 3.1.2 Scanning electron microscopy

The SEM images of the bare TiO<sub>2</sub>, Ag-deposited TiO<sub>2</sub> and EY-Ag/TiO<sub>2</sub> photocatalyst are shown in Fig. 3. It can be seen that the surfaces of the particles of EY-Ag/TiO<sub>2</sub> do not differ markedly from those the bare titania, being both rough and porous. The dark spots on the SEM micrograph are due to open pores on the surface of the catalysts. Estimated grain sizes from the figures show that the dye sensitized photocatalyst may have smaller particle size than regular TiO<sub>2</sub> photocatalyst.



### 3.1.4 Band gap determination

In order to determine the wavelength of light necessary for the excitation of the EY-Ag/TiO<sub>2</sub>, band gap energy was calculated from absorption data using Schuster-Kubelka-Munk's relational expression (Eq. 6).

$$[F(R)h\nu]^{1/n} = A(h\nu - E_g) \quad (6)$$

Where  $h$  is the Planck's constant,  $\nu$  is the frequency of vibration,  $\alpha$  is the absorption coefficient,  $E_g$  is the band gap and  $A$  is a proportionality constant.

If scattering is insignificant, the term  $h\nu\alpha$  is proportional to a function of reflectance  $[F(R)/h\nu]$ . Since the direct allowed sample transition is used in this experiment, the value of the denominator of the exponent  $n = 1/2$ . The bandgap corresponds to the intercept of the plot of  $(h\nu\alpha)^2$  or  $[F(R)h\nu]^2$  against  $h\nu$  (Fig. 5). The bandgap the EY-Ag/TiO<sub>2</sub> photocatalyst was found to be 3.06 eV (Fig. 5a) which stands in the vicinity of that of rutile TiO<sub>2</sub> (3.05 eV)<sup>41</sup>. A redshift is readily observed from the band gap of the commercial TiO<sub>2</sub> (3.25) (Fig. 5b) which shows that more of the visible light can now be absorbed by the sensitized photocatalyst.

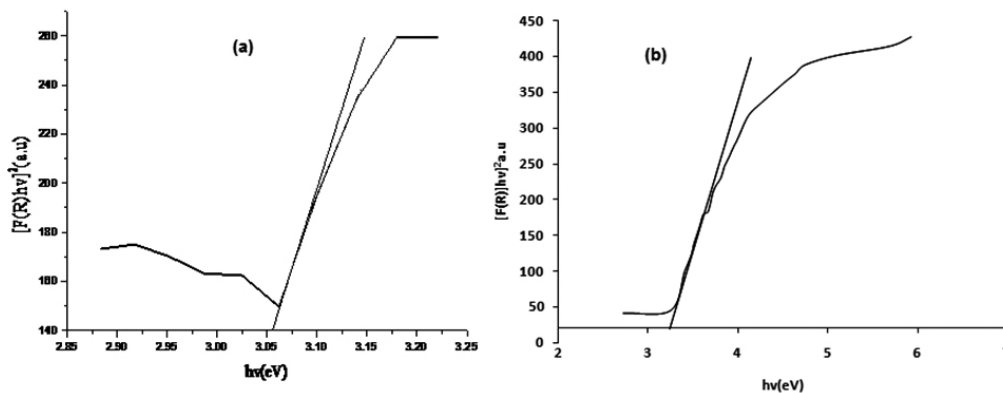


Fig. 5: Tauc's plot for (a) EY-Ag/TiO<sub>2</sub>, (b) Bare TiO<sub>2</sub>.

## 4.5 Optimizations of experiments

### 4.5.1 Amount of dopant in the catalyst

The effect of the amount of silver deposited EY-TiO<sub>2</sub> photocatalyst on the degradation of caffeine was studied in range of 0.3-2.1 % of Ag:Ti molar ratio (Fig. 6). The increase in the amount of the Ag load from 0.3 to 1.5% steadily

increases the photocatalytic degradation efficiency of caffeine. Decline in the degradation efficiency was observed at molar ratios above 1.5 %. Hence, the optimal Ag loading used in this study is 1.5%. This finding is in agreement with the study of photocatalytic degradation of methyl orange reported by Wen et al.<sup>27</sup> in which best degradation efficiency was obtained when TiO<sub>2</sub> was loaded with 1.6 % Ag.

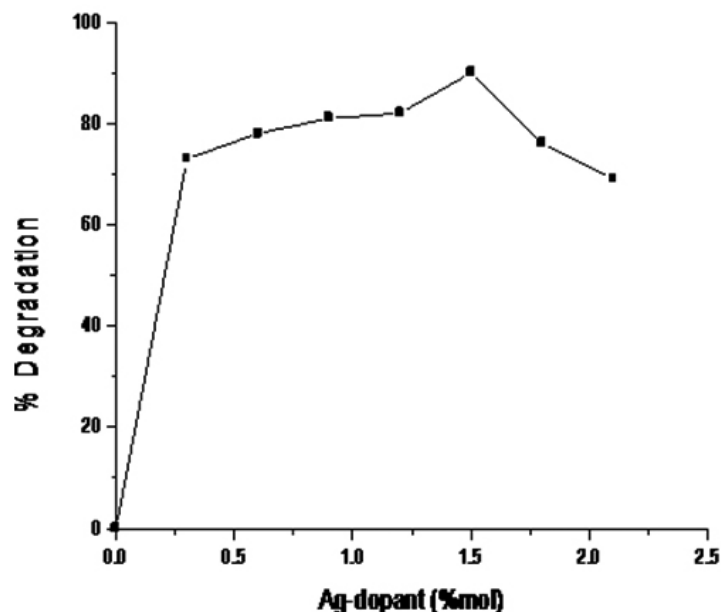


Fig. 6: Graph showing the effect Ag addition on the performance of the EY/Ag-TiO<sub>2</sub> catalyst.

### 4.5.2 Response surface methodology (RSM)

The values of degradation efficiency obtained from experiment (% D) were processed using response surface module to obtain statistically valid predicted values. These values for all the FCCD experiments are listed in Table 5. From the table it can be seen that there is good correlation between

the experimental and predicted degradation efficiencies as attested by linear normal plot of residuals (Fig. A-4, supplementary materials). Majority of the points on the normal probability plot lie roughly on a straight line, so it can be concluded that the estimated effects are the real and differ markedly from noise.

**Table 5:** Efficiency of different combination of levels of factors for caffeine removal.

Run	Factors			Degradation efficiency, % D	
	pH (A)	Catalyst (B; g/L)	Caffeine (C; mg/L)	(Experimental)	(Predicted)
1	3.0(-1)	2.5(+1)	50(+1)	50	53.15
2	8.0(+1)	2.5(+1)	50(+1)	82	76.05
3	8.0(+1)	1.75(0)	30(0)	90	78.20
4	8.0(+1)	2.5(+1)	10(-1)	92	107.35
5	3.0(-1)	1.75(0)	30(0)	44	65.80
6	3.0(-1)	2.5(+1)	10(-1)	74	63.45
7	8.0(+1)	1.00(-1)	10(-1)	87	81.35
8	5.5(0)	1.75(0)	30(0)	90	84.00
9	5.5(0)	1.75(0)	50(+1)	60	73.10
10	5.5(0)	1.75(0)	30(0)	73	84.00
11	5.5(0)	1.75(0)	30(0)	87	84.00
12	5.5(0)	1.75(0)	30(0)	95	84.00
13	3.0(-1)	1.00(-1)	10(-1)	76	79.45
14	5.5(0)	1.00(-1)	30(0)	76	81.00
15	5.5(0)	1.75(0)	30(0)	86	84.00
16	5.5(0)	1.75(0)	10(-1)	97	84.00
17	5.5(0)	2.5(+1)	30(0)	96	87.00
18	8.0(+1)	1.00(-1)	50(+1)	40	48.05
19	5.5(0)	1.75(0)	30(0)	80	84.00
20	3.0(-1)	1.00(-1)	50(+1)	85	67.15

The relationship between the degradation efficiency of caffeine (% D) under the interplay of the independent variables of the study A, B and C is best described by the reduced quadratic model described by equation (7), in which the quadratic contributions of catalyst and caffeine concentration terms vanish.

$$\% D = 84 + 6.2A + 3B - 10.9C - 12A^2 + 10AB - 5.25AC + 0.5BC \quad (7)$$

The response surface model was adjudged to be significant based on the analysis of variance (ANOVA) shown in Table 6. The model's Prob > F in the

table is less than 0.05 and this shows that predicted degradation efficiencies are not influenced at 95 % confidence level. Similarly, the Prob > F of 6.91 % for the lack-of-fit value indicates very low probability of occurrence due to noise.

**Table 6:** Analysis of variance for the response surface reduced quadratic model.

Source	Sum of squares	DF	Mean square	F-value	Prob > F	Remark
Model	3487.00	7	498.14	2.95	0.0479	Significant
<i>A</i>	384.40	1	384.40	2.28	0.1569	
<i>B</i>	90.00	1	90.00	0.53	0.4790	
<i>C</i>	1188.10	1	1188.10	7.05	0.0210	
<i>A</i> <sup>2</sup>	720.00	1	720.00	4.27	0.0611	
<i>AB</i>	882.00	1	882.00	5.23	0.0411	
<i>AC</i>	220.50	1	220.50	1.31	0.2751	
<i>BC</i>	2.00	1	2.00	0.012	0.9151	
Residual	2023.00	12	168.58			
Lack of Fit	1724.17	7	246.31	4.12	0.0691	Not significant
Pure Error	298.83	5	59.77			
Cor Total	5510.00	19				

Some measures of dispersion associated with the model of this study are listed in (Table A-1 of supplementary materials). From the Table, the PRESS value of the model of 17,967 indicates extremely high signal-to-noise ratio. The minimum adequate precision desirable in any experiment is a value > 4. In this study, the adequate precision is 7.221 which confirms adequate model

discrimination. The global effect of the operating variables are presented by the 3D response surfaces in Fig. 7. From Fig. 7a, there is synergy between catalyst concentration and pH as values as they are increased towards the intermediate levels (1.75 g/L and pH 5.5, respectively) and maximum degradation efficiency up to 87 % can be reached. The figure shows that alternating any of the

combinations of levels would result in low degradation efficiency. The same observation was made in the case of interplay of pH and caffeine concentration (Fig. 7b). However, in the case of catalyst and caffeine concentration (Fig.

7c), the degradation efficiency decreased as the amount of these variables is increased. This can be attributed to the screening of light by these parameters as their values are increased.

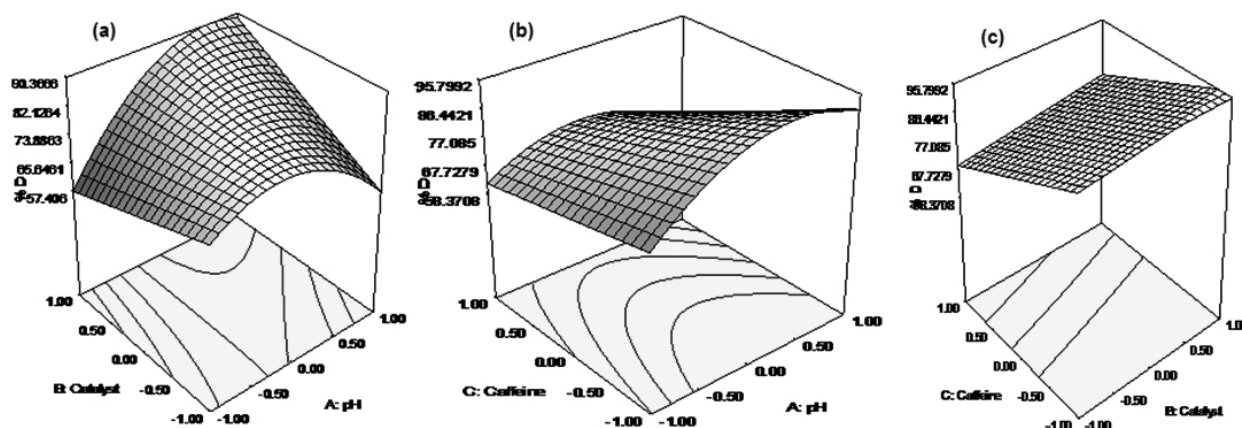


Fig. 7: Response surfaces for (a) pH and EY/Ag-TiO<sub>2</sub> concentration (b) pH and caffeine concentration (c) caffeine and catalyst concentration.

#### 4.5.3 Taguchi optimization of experiments

In this study, Taguchi design was also utilized for process optimization. The results of Taguchi method have the advantages of high reproducibility, reduced number of experiments and easy comprehension. Performance of set of variables the Taguchi experiments were measured based on signal-to-noise ratio, a response parameter that takes into account process mean and variance<sup>42</sup>. Experimental factors with signal to noise ratio larger than the mean effect were considered as the significant factors.

Table 7: Taguchi OA L<sub>9</sub> (3)<sup>4</sup> design Matrix.

Experiment	A	B	C	D	% Degradation
1	1	1	1	1	47
2	1	2	2	2	75
3	1	3	3	3	69
4	2	1	2	3	65
5	2	2	3	1	90
6	2	3	1	2	52
7	3	1	3	2	92
8	3	2	1	3	97
9	3	3	2	1	37

Table 7 shows the Taguchi design matrix consisting nine experiments at combination of three levels of four factors (EY-Ag-TiO<sub>2</sub> dose, A; pH, B; temperature, C and caffeine concentration, D) with each corresponding performance presented as percent degradation. The corresponding results of Taguchi experimental design are shown in Table 8. The influence of experimental factors was ranked based on the difference between the maximum and the minimum S/N ratios for a particular experimental factor, denoted as delta. Based on this, the order of influence is pH (B) > initial caffeine concentration (D) > EY/Ag-TiO<sub>2</sub> dosage (A) > temperature (C). In actual fact, it is well known that photocatalytic reactions are not affected by minor variations in temperature<sup>41</sup>. Similarly, the unrivalled dependence of the photocatalytic process on pH has variously been reported<sup>43</sup> as it affects the adsorption equilibrium. From Table 8, the optimal levels for each experimental factors obtained according to Taguchi's "the larger the better" criteria are accordingly, 2g/L catalyst dosage, pH 6, 45 °C temperature and 50 mg/L initial caffeine concentration. The optimum pH attained roughly matches the pH at point of zero charge of TiO<sub>2</sub> (pH<sub>pzc</sub> = 6.25)<sup>36</sup>. The implication is that pH will affect the adsorption equilibrium when exceedingly low or high resulting in poor degradation.

Table 8: Signal to noise (S/N) ratio response table for degradation of caffeine.

Level	A(g/L)	B	C(°C)	D(mg/L)
1	37.61	37.40	36.94	37.81
2	36.49	39.27	37.49	36.29
3	37.08	34.51	36.75	37.27
Delta	1.12	4.76	0.73	1.72
Rank	3	1	4	2

The influence of parameters in the degradation of caffeine can further be explained based on main effect. Main effect is considered present when the mean response changes across the level of experimental variables. The sign of the main effect indicates the direction of the effect. Fig. 8 shows that the temperature has negative effect on the photocatalytic degradation process whereas catalyst dosage and initial caffeine concentration have positive effect. Temperature has negligible consequence on the photodegradation kinetics because it has almost no contribution to the activation energy of TiO<sub>2</sub> due to its relatively high band gap<sup>41</sup>. Undoubtedly, increase in temperature might increase the kinetic energy of Eosin Y molecules, thus disrupting the sensitization linkages between EY molecules and TiO<sub>2</sub>. The positive effect of catalyst loading might be attributable to increase in the number of site available for generation of the free radicals responsible for the photodegradation process.

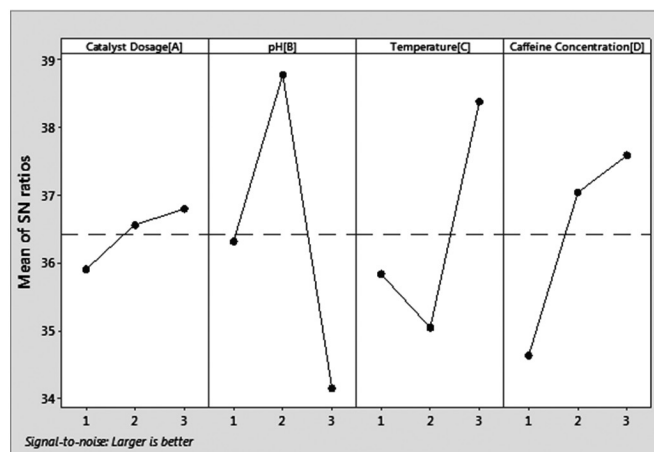


Fig. 8: Main effect plots for the S/N ratios depicting the effect of pH, catalyst dosage, temperature and initial concentration of caffeine.

The analysis of variance (ANOVA) (Table 9) was conducted to further investigate which design parameter significantly affects the degradation of caffeine. The p-value for each design parameter was chosen to dictate decisions as widely recommended. Examination of Table 9 suggests that temperature

has negligible influence in the rate of degradation of caffeine with the highest p-value of 0.8460 whereas pH, catalyst dosage and initial caffeine concentration with p-value of 0.005, 0.0195 and 0.0173, respectively, have significant effect on the degradation of caffeine, buttressing the order of effect described above.

**Table 9:** Results of the ANOVA for degradation of caffeine.

Source	DF	Adj SS	Adj MS	F-value	p-value
A	2	43.56	21.78	0.05	0.0195
B	2	2253.6	1126.78	14.68	0.0050
C	2	146.9	73.44	0.17	0.8460
D	2	270.2	135.1	0.33	0.0173

In order to corroborate the region where optimum response lies, contour plot (Fig. 9) was constructed using the most significant factors in the caffeine degradation (pH and caffeine concentration). The isolines on the contour plot represent distinct level of design parameter. The darker portion of the plot which is within the pH range of level 1 to 3 and catalyst dose of 2 to 3 g/L represent the area where there is highest probability of finding the optimum response (> 90 %). As seen from Fig. 9, the maximum of the contour plot is at level 2 for both the pH catalyst dosage. This indicates that at pH of 6 and catalyst dose of 1.5 gL<sup>-1</sup> the degradation efficiency will be greater than 90 %.

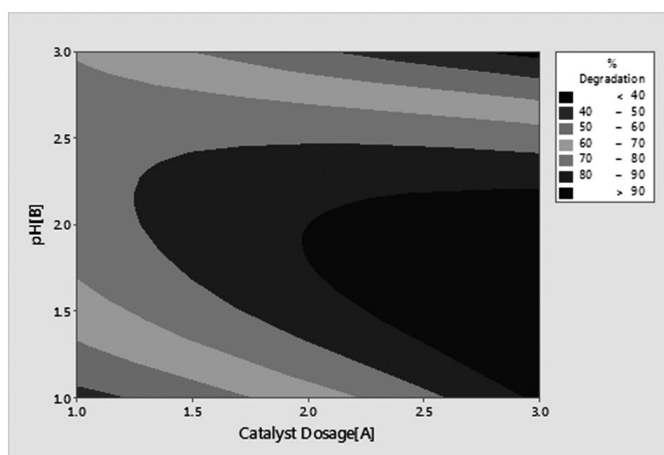


**Fig. 9:** Contour plot of percentage degradation versus pH and catalyst dosage.

#### 4.6 Kinetic scheme

The effect of photolysis and bare TiO<sub>2</sub> photocatalysis were studied and compared with the photocatalytic degradation profiles over EY/Ag-TiO<sub>2</sub>, Ag-doped TiO<sub>2</sub> and EY-sensitized TiO<sub>2</sub>. The results are displayed in Fig. 10. It can be observed from the figure that EY/Ag-TiO<sub>2</sub>, having 95 % removal at 290 min (Fig. 10d), has outperformed Ag-doped TiO<sub>2</sub> (52 % removal; Fig. 10b) and EY-sensitized TiO<sub>2</sub> (68%; Fig. 10c). As shown in Table 10, the caffeine degradation efficiency over the EY/Ag-TiO<sub>2</sub> is higher than that of titanium dioxide nanotube<sup>17</sup>. Moreover, unlike in the removal of caffeine by ozonation<sup>15</sup>, the degradation efficiency continued to steadily increase until almost all of the original caffeine has been removed. The bare-TiO<sub>2</sub> photocatalysis led to only 37 % caffeine removal (Fig. 10e) while irradiation alone was barely inefficient caffeine removal process (Fig. 10a).

Kinetic profiles based on pseudo zero-order and pseudo first-order integrated rate equations (Eq. 8 and 9, respectively) were plotted for experiments at optimum catalyst dosage (1.75 g/L), pH 5.5 and initial caffeine concentration (10 mg/L).

$$[\text{Caffeine}]_t = [\text{Caffeine}]_0 - k_o' t \quad (8)$$

$$\ln[\text{Caffeine}]_t = \ln[\text{Caffeine}]_0 - k_1' t \quad (9)$$

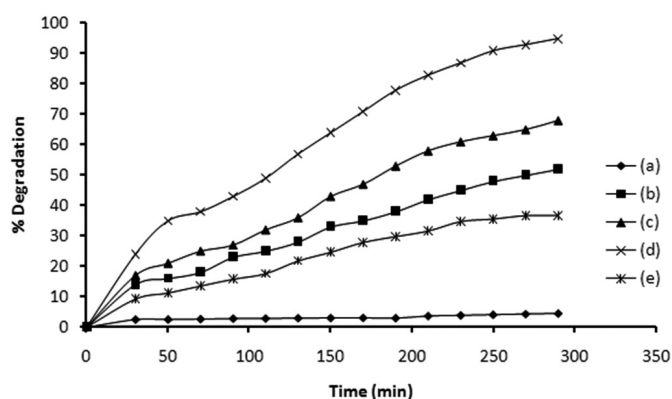


**Fig. 10:** Caffeine removal profiles under irradiation in presence of absence of catalyst (a) Irradiation alone (b) Ag-TiO<sub>2</sub> (c) EY-TiO<sub>2</sub> (d) EY/Ag-TiO<sub>2</sub> (e) TiO<sub>2</sub>.

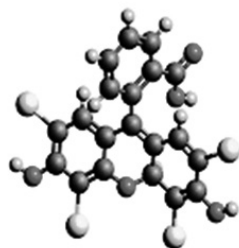
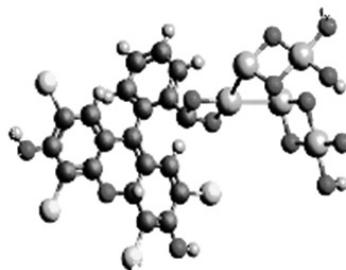
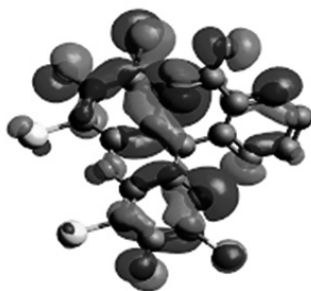
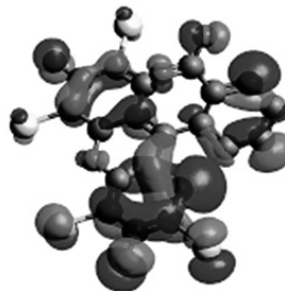
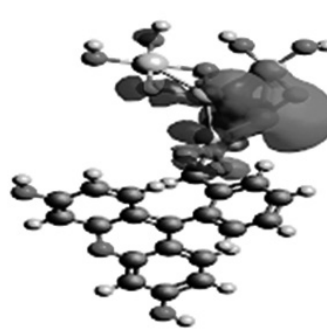
Where [Caffeine]<sub>t</sub> is the caffeine concentration at time t and [Caffeine]<sub>0</sub> is the initial caffeine concentration. The rate constant corresponding to each equation was obtained from the slope. Rate constant data obtained in this study is displayed by Table 10. The degradation of caffeine over EY-Ag/TiO<sub>2</sub> agreed with pseudo zero-order kinetic scheme with rate constant (k) of 1.7 x 10<sup>-2</sup> min<sup>-1</sup> (R<sup>2</sup> ≈ 0.99) (Fig. A-5, supplementary materials file). However we as usual with bare TiO<sub>2</sub> consistence with pseudo first-order scheme was observed as well as improved degradation efficiency upon downsizing from 138.64 nm to 69.32 nm (Fig. A-6, supplementary materials file). However, Barndök et al.<sup>44</sup> observed rather a decreased caffeine degradation efficiency with the downsizing of monodisperse anatase TiO<sub>2</sub> as shown in Table 10.

#### 4.6 Quantum chemical account of sensitization

In order to study the electron injection from dye to the TiO<sub>2</sub> and the energies associated with EY and EY sensitized TiO<sub>2</sub>, density functional theory calculations were carried out with the aid of the hybrid B3LYP functional, which integrates HF and Becke exchange terms with the Lee-Yang-Parr correlation functional by using 6-31G(d) basis set. The molecular structure of the optimized geometry of the EY and EY/TiO<sub>2</sub> are shown in Fig. 11a. The framework of the dye sensitized photocatalyst consists of Ti<sub>5</sub>O<sub>10</sub> cluster attached to the carboxylic acid group of the EY molecule via a bidentate bridge. The C10-C11 bonds of both the models are 1.34505-1.3942(Å) indicating the n-conjugation nature of the bonds. The calculated average Ti-O bond distance (1.97685 Å) is within the range reported by past workers (1.949 to 1.980 Å)<sup>46</sup>. The dipole moment of the EY/TiO<sub>2</sub> (8.2175 μ) is larger than that of EY (5.8244 μ) which indicates increased electronegativity due to the Ti-O bond.

**Table 10:** Kinetic parameters for EY/Ag-TiO<sub>2</sub> and TiO<sub>2</sub>.

Titania	Pseudo first-order			Pseudo zero-order			Ref.
	$k_f$ (10 <sup>-3</sup> mol dm <sup>-3</sup> s <sup>-1</sup> )	R <sup>2</sup>	%D	$k_z$ (10 <sup>-3</sup> min <sup>-1</sup> )	R <sup>2</sup>	%D	
EY/Ag-TiO <sub>2</sub> (69.32 nm)	3	0.956		1.7	0.988	95	This study
Bare TiO <sub>2</sub> (138.64)	6	0.965		1.5	0.934	37	This study
NF-TiO <sub>2</sub> (50 nm)	14.6	-	77	-	-		44
NF-TiO <sub>2</sub> (300 nm)	6.56	-	32	-	-		44
TiO <sub>2</sub> nanotube (10 nm)	-	-	51	-	-		17

**(a) Optimized geometry:****(i) EY****(ii) EY sensitized titania****(b) Frontier molecular orbitals of EY:****(i) HOMO****(ii) LUMO****(c) Frontier molecular orbital of Eosin yellow adsorbed on TiO<sub>2</sub>****(i) HOMO****(ii) LUMO****Fig. 11:** (a) Optimized geometry of Eosin Y and EY/Ag-TiO<sub>2</sub>, (b) Frontier molecular orbitals of Eosin Y (c) Frontier molecular orbitals of EY/Ag-TiO<sub>2</sub>.

The frontier molecular orbital of the EY and EY/TiO<sub>2</sub> are shown in Fig. 11b and Fig. 11c. As seen from the frontier molecular orbitals of the EY model, the electronic distribution of the HOMO and LUMO orbitals are delocalized over  $\pi$ -conjugation system of the three benzene rings and the highest electron density centered on the carboxylic acid functional group. The high electron density on the carboxyl functional group indicates the ease with which electrons can be injected to conduction band of the semiconductor photocatalyst. Generally speaking, for electrons to be effectively injected into the conduction band of the semiconductor photocatalyst, the LUMO eigenvalue of the dye molecule must be sufficiently more negative than the conduction band edge of TiO<sub>2</sub> (0.5 V) <sup>46</sup>. The eigenvalue for the HOMO and LUMO orbitals of the EY molecule were -0.24944 and -0.7246eV while for the Eosin Y-sensitized photocatalyst model these were -0.1511eV and -0.1827, respectively. It can be readily seen that, the energy gap ( $\Delta E$ ) between the HOMO and LUMO is larger in the case of the EY sensitized catalyst than the bare TiO<sub>2</sub> which implies the ease with which electrons can be injected into conduction band of the TiO<sub>2</sub> from the EY dye. The energy gap in the case of the sensitized catalyst is less than 0.5eV, thus falling within the range for molecules with unusual electronic properties such as intramolecular electron transfer in solution <sup>47</sup> and perhaps effective sensitization as in the present case.

**Table 11:** Excitation wavelength, energy and oscillator strength of main transition of EY and EY/Ag-TiO<sub>2</sub>.

Model	Wavelength (nm)	Energy(eV)	Oscillator strength (f)
EY	507	2.445759	0.1116
	412	3.009709	0.0928
	265	4.679245	0.0252
	247	5.020243	0.0061
EY-TiO <sub>2</sub>	844	1.469194	0.0071
	549	2.258652	0.0052
	426	2.910798	0.0375
	298	4.161074	0.0500

On the basis of optimized ground state geometries (Fig. 11a), absorption spectra of EY and EY-TiO<sub>2</sub> were calculated by DFT/B3LYP method. The results are shown in Table 11. The table shows the first optically excited transition of Eosin Y dye and Eosin Y-sensitized TiO<sub>2</sub> and the oscillator strength for singlet-singlet excitations. The most probable transitions were determined based on the value of the oscillator strength (f). Table 11 reveals the advantage of the sensitized TiO<sub>2</sub> to absorb over the range of 298 to 844 nm which predicts extended absorption beyond the visible region of the electromagnetic spectrum. This range brackets the wavelength of maximum absorption of EY (507 nm) determined in this study.

#### 4. CONCLUSION

Visible light photoresponsive catalyst with increased surface and reduced particle sizes was successfully synthesized by silver doping and dye sensitization of a commercial TiO<sub>2</sub> brand. The degradation of caffeine over this catalyst was remarkable (97%), but pH constrained. The sensitization of Ag-TiO<sub>2</sub> resulted in amorphousness and downsizing of the precursor TiO<sub>2</sub> particles. Results showed the capacity of the catalysts to absorb the entire range of visible light spectrum.

#### ACKNOWLEDGEMENT

Muktar Ibrahim thankfully acknowledges the constructive criticisms of members of Gaya's research group of the Department of Pure and Industrial Chemistry, Bayero University, Kano, during his days as student.

#### REFERENCES

- [1] C. Indermuhle, M.J. Martín de Vidales, C. Sáez, J. Robles, P. Cañizares, J.F. García-Reyes, A. Molina-Díaz, C. Cominellis, M.A. Rodrigo, *Chemosphere* **93**, 1720, (2013)
- [2] H.J. Souza, C.B. Moyses, F.J. Pontes, R.N. Duarte, C.E. Sanches da Silva, F.L. Alberto, U.R. Ferreira, M.B. Silva, *Mol. Cell. Probes* **25**, **231**, (2011)
- [3] C. Xu, L. Chen, L. You, Z. Xu, L.F. Ren, K.Y.-H. Gin, Y. He, W. Kai, *Environ. Sci.: Processes Impacts* **20**, 1030, (2018)
- [4] S. Weigel, J. Kuhlmann, H. Hühnerfuss, *Sci. Total Environ.* **295**, 131, (2002)
- [5] W.A. Cabrera-Lafaurie, F.R. Román, A.J. Hernández-Maldonado, *J. Hazard. Mater.* **282**, 174, (2014)
- [6] O.M. Couto Jr, I. Matos, I. Maria da Fonseca, P.A. Arroyo, E. Antônio da Silva, M.A.S. Dornellas de Barros, *Can. J. Chem. Eng.* **93**, 68 (2015)
- [7] L.P. Padhye, H. Yao, F.T. Kung'u, C.-H. Huang, *Water Res.* **51**, 266, (2014)
- [8] P. Wang, Z. Guan, Q. Li, J. Yang, *J. Mater. Sci.* **53**, 774, (2017)
- [9] R. Rosal, A. Rodríguez, J.A. Perdigón-Melón, A. Petre, E. García-Calvo, M.J. Gómez, A. Agüera, A.R. Fernández-Alba, *Chemosphere* **74**, 825 (2009)
- [10] O. Ganzenko, N. Oturan, D. Huguenot, E.D. van Hullebusch, G. Esposito, M.A. Oturan, *Water Res.* **156**, 987, (2015)
- [11] A.O. Ibhadon, F.H. Paul, *Catalysts* **3**, **234**, (2013)
- [12] N. Nakada, H. Shinohara, A. Murata, K. Kiri, S. Managaki, N. Sato, H. Takada, *Water Res.* **41**, 4373, (2007)
- [13] N. Vieno, T. Tuhkanen, L. Kronberg, *Water Res.* **41**, 1001, (2007)
- [14] M. Klavarioti, D. Mantzavinos, D. Kassinos, *Environ. Int.* **35**, 402, (2009)
- [15] R. Rosal, A. Rodríguez, J.A. Perdigón-Melón, A. Petre, E. García-Calvo, M.J. Gómez, A. Agüera, A.R. Fernández-Alba, *Chemosphere* **74** (2009) 825–831. <https://doi.org/10.1016/j.chemosphere.2008.10.010>.
- [16] U.I. Gaya, *Heterogeneous Photocatalysis Using Inorganic Semiconductor Solids*, Springer, Dordrecht, 2014.
- [17] M.K. Arfanis, P. Adamou, N.G. Moustakas, T.M. Triantis, A.M. Kontos, P. Falaras, *Chem. Eng. J.* **310**, 525, (2017)
- [18] J. Matos, B. Llano, R. Montaña, P.S. Poon, M.C. Hidalgo, *Environ. Sci. Pollut. Res.* **25**, 18894, (2018)
- [19] P. Chowdhury, J. Moreira, H. Gomma, A.K. Ray, *Ind. Eng. Chem. Res.* **51**, 4523, (2012)
- [20] X. Li, J.-L. Shi, H. Hao, X. Lang, *Appl. Catal., B.* **232**, 260, (2018)
- [21] D. Chatterjee, A. Mahata, *J. Photochem. Photobiol. A.* **165**, 19, (2004)
- [22] M. Grätzel, *Inorg. Chem.* **44**, 6841, (2005)
- [23] S. Rengaraj, X.Z. Li, *J. Mol. Catal. A: Chem.* **243**, 60, (2006)
- [24] H. Ran, J. Fan, X. Zhang, J. Mao, G. Shao, *Appl. Surf. Sci.* **430**, 515, (2017)
- [25] P. Wang, L. Zong, Z. Guan, Q. Li, J. Yang, *Nanoscale Res. Lett.* **1**, (2018)
- [26] A. Yusuf, U. Gaya, *Nanochem. Res.* **3**, 29, (2018)
- [27] R.A. Spurr, H. Myers, *Anal. Chem.* **29**, 760, (1957)
- [28] K.P.D.A. Savio, D. Starikov, A. Bensaoula, R. Pillai, L.L. de La Torres Garcia, C.R. Hernández, *Ceram. Int.* **38**, 3529 (2012)
- [29] Y. Zhang, Q. Li, *Solid State Sci.* **16**, 16, (2013)
- [30] K. Lalitha, J.K. Reddy, M.V.P. Sharma, V.D. Kumari, M. Subrahmanyam, *Int. J. Hydrogen Energy* **35**, 3991, (2010)
- [31] L. Wen, B. Liu, C. Liu, X. Zhao, *Journal of Wuhan University of Technology-Mater. Sci. Ed.* **24**, 258, (2009)
- [32] K. Selvam, M. Swaminathan, *J. Mol. Catal. A: Chem.* **351**, 52, (2011)
- [33] S. Sakthivel, M.V. Shankar, M. Palanichamy, B. Arabinthoo, D.W. Bahnemann, V. Murugesan, *Water Res.* **38**, 3001, (2004)
- [34] M. Nag, D. Guin, P. Basak, S.V. Manorama, *Mater. Res. Bull.* **43**, 3270, (2008)
- [35] K. Selvam, M. Swaminathan, *RSC Adv.* **2**, 2848, (2012)
- [36] M.R. Hoffmann, S.T. Martin, W. Choi, D.W. Bahnemann, *Chem. Rev.* **95**, 69, (1995)
- [37] D.A.H. Hanaor, C.C. Sorrel, *J. Mater. Sci.* **46**, 855, (2011)
- [38] B. Ohtani, *J. Photochem. Photobiol. C.* **11**, 157, (2010)
- [39] B. Ohtani, *Chem. Lett.* **37**, 217, (2008)
- [40] J. Coates in *Encyclopedia of Analytical Chemistry*, R.A. Meyers eds., Wiley & Sons Ltd, Chichester, 2000; pp.10815-10837.
- [41] O. Carp, C.L. Huisman, A. Reller, *Prog. Solid. State Chem.* **32**, 33, (2004) *Eng. J.* **310**, 525, (2017)
- [42] I. Asiltürk, H. Akkuş, *Measurement* **44**, 1679, (2011)
- [43] R.R.N. Marques, M.J. Sampaio, P.M. Carrapi, C.G. Silva, T.S. Morales, G. Drazic, J.L. Faria, A.M.T. Silva, *Catal. Today* **209**, 108, (2013)
- [44] H. Barndök, M. Peláez, C. Han, W.E. Platten III, P. Campo, D. Hermosilla, A. Blanco, D.D. Dionysiou, *Environ. Sci. Pollut. Res.* **20**, 3582, (2013)
- [45] S.-D. Mo, W.Y. Ching, *Phys. Rev. B: Condens. Matter Mater. Phys.* **51**, 13023, (1995)
- [46] C. Dette, M.A. Pérez-Osorio, C.S. Kley, P. Punke, C.E. Patrick, P. Jacobson, F. Giustino, S.J. Jung, K. Kern, *Nano Lett.* **14**, 6533, (2014)
- [47] D.F. Perepichka, M.R. Bryce, *Angew. Chem. Int. Ed.* **44**, 5370, (2005)